Rensselaer

December 24, 1991

Dr. Edwin P. Rood
Office of Naval Research
Scientific Office Code-1132F
800 North Quincy Street
Arlington, VA 22217-5000

Dear Dr. Rood:

The purpose of this letter is to transmit the fourth quarterly report for ONR grant N00014-91-J-1271, "An Experimental Study of Plunging Liquid Jet Induced Air Carryunder and Dispersion" (Lahey & Drew - CoPI).

This report period was devoted to taking plunging liquid jet data, in which a conical nozzle was used. The DANTEC LDA/PDA system was used to acquire these data, and flow visualization was performed using a Kodak high speed video system (some output of which I have sent to you on November 25, 1991).

The results of this study have been documented in the enclosed technical paper entitled, "An Experimental Study on Air Carryunder Due to Plunging Liquid Jets". This paper will be sent to the *International Journal of Multiphase Flow* for consideration for publication.

It can be seen in the data reported in the enclosure, that the air carryunder is due to an instability in an annular shaped sheet of air which is induced in the liquid pool because of the drag of the plunging liquid jet. By the end of the report period work was underway to perform a stability analysis of the breakup of the induced air sheet. It is intended that the results from this analysis will provide the initial condition for a three-dimensional two-phase jet dispersion analysis using PHOENICS. That is, this analysis will hopefully provide a way of quantifying the amount of air entrained and the initial bubble size distribution.

Preliminary analysis using PHOENICS 1.4 has indicated that a standard k-ε turbulence model is insufficient to accurately determine jet spreading, even for single-phase jets. As a consequence, the turbulence modeling is currently being improved and benchmarked against well known data and/or analytical results.

In addition, Ms. Margo Frommeyer (ONR POPS representative, 601-688-5213) has been contacted about getting CRAY YMP-8 computer time for this project, and Ms. Samantha Breedin (601-688-7677, Stevens Space Center) has agreed to mount PHOENICS 1.6 on their computer once I have a valid POPS use account. Also, Ms. Paula Cranage (CHAM-U.K.) has agreed to provide PHOENICS 1.6 to Ms. Breedin, at no charge, once everything is set).

Once PHOENICS is operational it should be possible to implement a state-of-the-art three-dimensional two-fluid bubbly flow model into it, such that detailed calculations of two-phase jet spreading can be performed. I trust that there will not be too much more delay in getting my POPS account established.

If you have any questions concerning this letter or the enclosure, please contact me or Professor Drew directly [Lahey: 518-276-8579; Drew: 518-276-6903].

Sincerely yours,

Dr. R.T. Lahey, Jr.
The Edward E. Hood, Jr. Professor of Engineering

RTL/ev
Attachment

cc:
- Administrative Grants Officer - ONR
- Director - Naval Research Laboratory
- Defense Technical Information Center
- D.A. Drew (RPI)
- F. Bonetto (RPI)

AN EXPERIMENTAL STUDY ON AIR CARRYUNDER DUE TO A PLUNGING LIQUID JET

F. Bonetto
R.T. Lahey, Jr.
Rensselaer Polytechnic Institute
Troy, NY 12180-3590 USA

INTRODUCTION

A good understanding of the air carryunder and bubble dispersion process associated with a plunging liquid jet is vital if one is to be able to quantify such diverse phenomena as the environmental impact of power plant discharges, sea surface chemistry, the meteorological significance of (breaking) ocean waves, the performance of certain type of chemical reactors, the "greenhouse" effect (ie, the absorption of CO_2 by the oceans), and a number of other important maritime-related applications. In particular, the air entrainment process due to the breaking bow waves of surface ships may cause long (ie, up to 5 km in length) wakes. Naturally easily detectable wakes are undesirable for naval warships.

A number of prior studies have been performed in which axisymmetric plunging jets have been used to investigate the air carryunder process. These include the work of Lin & Donnelly [1966], Burgess et al [1972], Van De Sande & Smith [1973], Koga [1982], McKeogh & Ervine [1981], and Detsch & Sharma [1991].

Unfortunately, in most of these experiments only global measurements were made. While such measurements may allow one to correlate an onset-of-air-carryunder criteria, they provide very limited information on the fluid mechanics of bubble entrainment and the resultant dispersion process in the induced two-phase jet.

In the present study plunging liquid jet experiments were performed and detailed Laser Doppler Anemometer (LDA) data were taken of the phasic velocity field and the void fraction distribution in the induced two-phase jet.

EXPERIMENTAL SETUP

As shown in Figure-1, a converging nozzle oriented vertically produced an axisymmetric liquid (ie, water) jet. This jet impacted at 90° a pool of water and, when a threshold velocity was exceeded, it was observed that the plunging liquid jet caused air entrainment. In agreement with the observations of McKeogh & Ervine [1981], different two-phase jet characteristics were noted, depending on the turbulence intensity of the plunging liquid jet. For a laminar liquid jet (ie, one having a turbulence intensity less than about 0.8%) the diameter of the induced bubbles were in the range 2-300 μm. On the other hand, for a liquid jet turbulence intensity of about 3%, the entrained bubbles had diameters in the range of 1-3 mm.

Figure 1 shows a schematic of the test loop. A screw pump was used to force the water through the nozzle as well through a bypass. The pump had a speed controller which was used to make the coarse control of the liquid flow rate through the nozzle. In the bypass a valve was used for the fine control of liquid flow rate. In order to damp out any flow oscillations, an accumulator was placed on the discharge side of the pump.

The acrylic conical nozzle, shown schematically in Fig. 2, consisted of an arrangement of honeycombs and screens followed by a smooth contraction. In this way the turbulence level of the liquid jet could be parametrically varied. The exit diameter of the nozzle was 4.76 mm, and this produced a liquid jet which was about 5.1 mm in diameter. The acrylic tank which contained the water pool had dimensions $0.914 \times 0.916 \times 1.465 = 1.265$ m^3. The suction of the tank was put as far from the liquid jet impact point as possible in order to minimize the influence of this flow on the two-phase jet's flow.

A DANTEC Fiber-Flow Laser Doppler Anemometer (LDA) system was used to nonintrusively measure the liquid and gas velocities (both the mean and

fluctuations). This system consisted of submersible transmitting and receiving optics.

The transmitting optics were powered by a 10 W Ar-ion laser. The laser beam was split into two beams, where one beam passed through a Bragg cell to produce a fringe shift of 40 MHz in the measurement volume. Optical fiber wave guides conducted the laser beams to the submersible LDA heads. A 600 mm focal length lens was used in these experiments. A beam expander was also used to reduce the size of the measurement volume and increase the light intensity.

The receiving optics was used in a back-scattering configuration. Optical fibers conducted the scattered light to the photomultipliers after the light was optically filtered. The photomultipliers converted the optical signal into an electrical signal that was processed by a special covariance signal processor. An AT micro-computer collected and processed the data.

The receiving optics used for the smooth jet employed a Fiber Particle Dynamic Analyzer (FPDA) system with 600 mm focal length lenses and a special aperture plate to maximize the bubble size range. The axial velocity of the liquid jet was used as the master signal for data collection. The collected light was transmitted through three optical fibers to a special FPDA device having three photodetectors for bubble size measurement.

The signals collected by the AT computer consisted of the:

- arrival time of the particles
- transit time of the particles
- velocity of the particles
- equivalent diameter of the particles

Two different methods were used for the measurement of void fraction in the two-phase jet: a KfK impedance probe and the particle time fraction from the FPDA. The impedance probe consists of two electrically isolated electrodes; one at

the tip of the probe and another upstream electrode which is always in contact with the liquid in the pool. The liquid (ie, water) has a relatively high electrical conductivity and thus when the tip is in contact with the liquid a relatively high current flows through to a Wheatstone bridge circuit. The difference between the conductivities of the liquid and gas phases produces a different signal depending on whether there is liquid or gas present at the tip of the probe. The active element of the probe's tip was 150 μm in diameter and it was calibrated with bubbles having diameters in the 1-3 mm range. This type of probe is a standard tool used for measuring void fraction in air/water bubbly flows [Hewitt, 1978].

The KfK impedance probe was used to measure the void fraction in the rough jet (which had bubbles of diameter in the range 1-3 mm) because the size of bubbles produced was out of range of the FPDA (ie, the air bubbles were too large for the lens size used). In contrast, for the measurement of void fraction when a smooth liquid jet was tested, the impedance probe could not be used because the size of the bubble were the same order of magnitude as the size of the tip (ie, the air bubbles were quite small). However, the FPDA could be, and was, used to measure the size distribution of the bubbles in this case.

A particle crossing the control volume of the LDA with a velocity u perpendicular to the LDA fringes produces light modulation in the photomultiplier that has a Doppler frequency of:

$$f_D = \frac{2u}{\lambda} \sin\left(\frac{\theta}{2}\right) \tag{1}$$

where

λ = wavelength of the laser light

θ = angle between the laser beams

u = particle velocity component perpendicular to the fringes

f_D = Doppler frequency

An effect discovered by Mie is that if instead of using the output of one photomultiplier, one uses the outputs of two photomultipliers in spherical coordinates (ϕ,ψ) there is a phase difference between the signals produced by the two photomultipliers. This phase difference, Θ, is given by:

$$\Theta = \pi \frac{d\,n}{\lambda} \sqrt{2} \left\{ \left(1 + \sin\frac{\theta}{2} \sin\phi \sin\psi - \cos\frac{\theta}{2} \cos\phi \right)^{1/2} - \left(1 - \sin\frac{\theta}{2} \sin\phi \sin\psi - \cos\frac{\theta}{2} \cos\phi \right)^{1/2} \right\} \quad (2)$$

where

n = index of refraction of the medium

d = particle diameter

Durst [1975] was apparently the first to use this principle to measure the diameter of particles. Although Durst measured the diameter of relatively large particles (ie, 2 mm in diameter) his method was extended to the μm range by Buchhave.

The measurement system used in this work had three photomultiplier with the proper geometrical configuration to have broad band dynamical response. The phase difference between photomultipliers 1 and 2 was used to estimate the diameter subrange of the particles. The phase difference between photomultipliers 2 and 3 was then used to evaluate the diameter of the particle more accurately. The phase difference between photomultipliers 1 and 3 gave a consistency check (ie, it was verified that the sum of the three phase differences was 2π).

The FPDA was calibrated using a suspension of polystyrene particles which had a diameter of 9 5 μm + 0.5 μm, and a steel ball of diameter 0.4 mm.

The LDA/FPDA system and the KfK impedance probe were mounted on a Benjamin Systems three-dimensional traversing mechanism having a 1 μm positioning resolution. The tip of the KfK impedance probe was 0.3 mm under the measurement volume of the LDA/FPDA system for void fraction measurements when a rough jet liquid was tested.

The turbulence intensity of the liquid jet at the nozzle exit was found to be one of the most important parameters affecting jet roughness and the size of the bubbles entrained by the plunging liquid jet. An arrangement of honeycombs and screens were used to control the turbulence intensity of the flow entering the conical nozzle. The attenuation of the turbulence due to the screens and honeycombs is given by

$$f = \frac{1}{1+K} \qquad \text{Axial reduction [Prandtl, 1933]}$$

$$f = \frac{1}{(1+K)^{1/2}} \qquad \text{Lateral reduction [Dryden, 1947]} \qquad (3)$$

where,

K is the pressure loss coefficient (in velocity heads)

Downstream of the honeycombs and screens the liquid flowed through an axisymmetric contraction. Prandtl [1933] showed that the attenuation of the turbulence in a convergent nozzle is:

$$f = 1/C^2 \qquad \text{Axial reduction}$$

$$f = 1/C^{1/2} \qquad \text{Lateral reduction} \qquad (4)$$

where C is the area contraction ratio.

It was found that Eqs. (3) and (4) somewhat overpredicted the attenuation of the turbulence. In the next section the results for a liquid jet with a turbulence

intensity of $u_\ell'/\bar{u}_\ell = 0.8\%$ are presented. From now on this level of turbulence will be referred to as the "smooth jet". Later the results for a liquid jet with a turbulence intensity of $u_\ell'/\bar{u}_\ell = 3\%$ will be presented. This level of turbulence was found to produce a visibly "rough jet".

EXPERIMENTAL RESULTS - SMOOTH JET

It was found that the best nozzle configuration to minimize the turbulence intensity of the jet at the nozzle exit was as follows:

(1) Two honeycombs separated by one half tube (inner) diameter, with the first honeycomb placed right after the nozzle inlet.

(2) Two grids separated one tube (inner) diameter apart. The first grid was a distance of half tube (inner) diameter from the last honeycomb.

A high speed Kodak video camera with a zoom lens was used to visualize the induced two-phase flow. As shown schematically in Fig-3, we observed that an annular meniscus was formed adjacent to where the jet impacted the liquid pool. Within this meniscus, a thin annular sheet of air was induced because of the drag of the liquid jet. This sheet of air became unstable leading to the entrainment of air bubbles. Near the surface, we did not observe bubbles, rather the air was present only in the thin annular sheet. This agrees with previous observations [Detsch & Sharma, 1991]. Due to breakup of the annular sheet, air carryunder ooccurred. The entrained bubbles were dispersed and a spreading two-phase jet developed with the gas (ie, dispersed) phase present in a conical configuration.

The FPDA system was focused on the centerline of the jet at a distance from the undisturbed free surface of the pool of z = 35.1 mm. The liquid jet's flow rate was w = 0 143 kg/s, and the distance from the nozzle exit to the surface of the liquid pool was h = 9.0 mm. Figure 4 shows the probability density function for

particle size. It can be seen that the distribution has a maximum for a bubble diameter of about 156 μm. Also, there is a pronounced peak for very low values of particle diameter. From this FPDA signal alone it was not possible to determine if the spike at the smallest diameter was produced only by liquid seeding. That is, seeding of the liquid was done using polystyrene particles having 9.5 μm mean diameter, and the particles inherent in the tap water which was used.

In order to better understand the origin of this peak an experiment was run in which the liquid jet's mass flow rate was slightly lower than the threshold value for air entrainment. For this situation we measured only the liquid seeding signals, because there was no air entrainment. Next, we set the liquid flow rate through the nozzle to a value slightly exceeding the threshold for air entrainment. With this configuration we had approximately the same liquid seeding signals and we also had the signals produced by any small bubbles. The histogram with seeding particles only had the same shape as the sharp peak at the lowest size shown in Figure-4, however the data rate was approximately 10% of the data rate produced by the particles having diameters less than 20 μm for the case in which we were entraining air. The conclusion is that the liquid seeding signals contribute to this peak but they do not account for all the particles measured. In particular, there was a significant number of air bubbles having a diameter less than 20 μm.

Figure 5 shows the probability density function of the liquid phase velocity. The first order moment of the distribution (ie, the rms fluctuation) is defined as,

$$u_\ell'^2 = \frac{1}{n-1} \sum_i (u_{\ell i} - \bar{u}_\ell)^2 \qquad (5)$$

The corresponding value of u_ℓ' corresponding to Fig-4 was 1.18 m/s. Interestingly, this is approximately equal to the u_ℓ' corresponding to the single-phase flow value

for the same position and liquid jet flow rate. This was characteristic of the smooth jet behavior, and indicates that bubble-induced turbulence was very small compared to the shear-induced turbulence in the liquid phase.

The transit time (i.e., the residence time) of the particle in the measurement volume was also collected. A correlation between the transit time of a particle and its size and velocity was found. Moreover, it was found that using the information on the velocity and the transit time one could predict if the bubbles have a size similar to the seeding particles or if they were larger. However the velocity and transit time information alone was not enough to accurately calculate the bubble size. This fact can be easily understood if we suppose that the particles are much bigger than the measurement volume. Then the transit time is a function of the chord length of the particle and its velocity. In the best case the chord length can be calculated but this is not normally the bubble diameter. Thus the transit time information could be used to sort between the liquid and gas velocities but could not be used for bubble size measurement.

The slip ratio (S) between the liquid and the gas was found to be near unity for the relatively small bubbles associated with a smooth liquid jet. It was somewhat lower than unity because in two-phase jet downflow the gas velocity was lower than the liquid velocity due to buoyancy.

It was found that the bubbles with diameters smaller than 20 μm traveled at the liquid phase velocity, while bubbles having diameters bigger than 20 μm were at a velocity which was somewhat less than the local liquid velocity.

Figure 6a depicts a contour plot of the two-dimensional probability density function of the particle diameters (d_p) and axial velocities (u_z). The plots are the curves of constant counts for the same conditions as in Figs-4 & 5. Quantitatively the most probable value of peak #1 was at, d_p = 5 μm, u_z = 4.05 m/s, and the most probable value of peak #2 was at d_p = 125 μm, u_z = 3.5 m/s.

Figure-6a indicates that the velocity of the bubble was not dependent on its size. If the velocity of the bubbles had changed with size we would see the iso-count curves with their principal axes forming an angle with the horizontal. There is no such trend seen in Figure 6a.

Figure 6b presents the same information as in Fig-6a. For a given bubble diameter it shows the average axial bubble velocity u_z (continuous line) and the rms fluctuation u_z' (ie, the error bars). It can be clearly seen that the mean axial bubble velocity does not depend on bubble diameter.

EXPERIMENTAL RESULTS - ROUGH JET

Figure 7 shows the liquid velocity histogram at the centerline of the liquid jet for a flow rate of w = 0.144 kg/s, a distance from the nozzle to the undisturbed pool surface of h = 29.9 mm, and a distance from the pool surface to the measurement volume of z = 33 mm. The mean axial velocity is u_ℓ = 4.96 m/s. One of the main differences between a rough liquid jet and a smooth jet is that in the latter case the liquid flow field is practically unaffected by the bubbles while in the former, the bubbles are much larger, thus the discrete phase increases the continuous phase's turbulence intensity. This also increases the phasic momentum exchange resulting in greater dispersion of the two-phase jet and a lower velocity of the liquid velocity.

Figure 8 depicts the histogram of the gas velocity for the same conditions as Fig-7. There is a significant difference between the mean values of the liquid velocity and the gas velocity, and this was generally true for the rough liquid jet data. The slip ratio in this case was less than for the smooth jet due to the larger buoyancy associated with the bigger entrained bubbles.

Figure 9 presents the liquid and gas velocity as a function of radial position (r) for h = 17.3 mm, w_ℓ = 0.125 kg/s and z = 50.0 mm. It was found that the two-

phase jet was more dispersed than the corresponding single-phase flow case and that the turbulence intensity was higher. This turbulence enhancement is due to bubble-induced turbulence. In this case the bubble-induced turbulence accounts for about 30% of the total turbulence level.

Figure 10 shows for w_ℓ = 0.181 kg/s, h = 30 mm and r = 0 (ie, on the jet's centerline) the local void fraction, which is defined as the time fraction,

$$\alpha = \sum_i \Delta t_i / T \tag{6}$$

As discussed previously, a KfK impedance probe was used for these void fraction measurements. A post-processing of the properly thresholded signals was used to evaluate the local void fraction. The axial location z = 0 in Fig-10 corresponds to the point of impact of the liquid jet if the pool surface was undisturbed under the centerline of the liquid jet (ie, at r=0). The value of the local void fraction at this point was zero because only liquid was present. As the measurement volume was moved down (ie, z > 0) bubble carryunder and dispersion occurs which causes the local void fraction at r = 0 to increase with z. A competing mechanism that causes the void fraction to later decrease is that the two-jet spreads as we increase z. In the case shown the maximum void fraction on the jet's centerline (r = 0) is at z = 42 mm.

As noted previously, when the liquid impacts the pool surface, air entrainment occur around the jet's circumference. In Figure 11 we have the local void fraction as a function of r and z. We see that the void fraction has a maximum at $r = d_{jet}/2 \cong 2.5$ mm. We note that at first the local void fraction builds up, then void dispersal occurs as the two-phase jet spreads. In the high speed video of our experiments the event of having bubbles at the liquid jet's centerline

for $z < 10$ mm was very rare. Also, it can also be observed in Fig-11 how the two-phase flow jet disperses as z increases.

Interestingly, off-centerline peaking of void fraction was not in the data of McKeogh & Ervine [1981] for similar conditions (ie, $u'_\ell / \bar{u}_\ell = 5\%$, $d_{jet} = 9$ mm, $w_\ell = 0.199$ kg/s). This is presumably because the data presented herein is based on detailed local measurements.

Figure 12 depicts the void fraction as a function of distance from the nozzle to the water level, h, for $z = 35$ mm, $w_\ell = 0.127$ kg/s and $r = 0$ (ie, on the centerline of the liquid jet). The effect of air carryunder is clearly seen.

SUMMARY AND CONCLUSIONS

New detailed LDA/FPDA data has been taken of the air carryunder process associated with a plunging liquid jet. It has been found that the amount and bubble size of the air entrained depends on the level of turbulence (ie, roughness) of the liquid jet.

These data provide the insights necessary for the development of analytical models of the air entrainment process. Moreover, they should also be useful for benchmarking phenomenological or mechanistic Computational Fluid Dynamic (CFD) analysis of the dispersion process in the induced two-phase jet.

ACKNOWLEDGMENT

The financial support of this study by the Office of Naval Research (ONR) is gratefully acknowledged.

REFERENCES

Burgess, J.M., Molloy, N.A. and McCarthy, M.J., "A Note on the Plunging Liquid Jet Reactor," *Chem. Eng. Sci.*, Vol. 12, 442, 1972.

Detsch, R. and Sharma, R.N., "The Critical Angle for Gas Bubble Entrainment by Plunging Liquid Jets," to be published, *Chem. Eng. J.*, 1991.

Dryden, H.L. and Schuabauen, G., "The Use of Damping Screens for the Reduction of Wind Tunnel Turbulence," JAS, 14, pp. 221-228, April 1947.

Durst, F., Eliasson, B., "Properties of Laser Doppler Signals and Their Exploitation for Particle Size Measurements," Proc. LDA Symp., Copenhagen, 1975, pp. 115-137.

Hewitt, G.B., *Measurement of Two-Phase Parameters*, Academic Press, 1978.

Koga, M., "Bubble Entrainment in Breaking Wind Waves," *Tellus*, Vol. 34, 481, 1982.

Lin, T.J. and Donnelly, H.G., "Gas Bubble Entrainment by Plunging Laminar Liquid Jets," *AIChE Journal*, Vol. 12, No. 3, 563, 1966.

McKeogh, E.J. and Ervine, D.A., "Air Entrainment Rate and Diffusion Pattern of Plunging Liquid Jets," *Chem. Eng. Sci.*. Vol. 36, 1161, 1981.

Moral, T., "Design of Two-Dimensional Wind Tunnel Contractions," *J. Fluids Eng.*, pp. 371-378, 1977.

Prandtl, L., "Attaining a Steady Air Stream in Wind Tunnels," NACA TM 726, October 1933.

Rae, W. and Pope, A., *Low Speed Wind Tunnel Testing*, 2nd Ed., Wiley-Interscience, 1984.

Scheiman, J. and Brooks. J.D., "Comparison of Experimental and Theoretical Turbulence Reduction from Screens, Honeycombs, and Honeycomb-Screen Combinations," JAS, 18, 638-643, August 1981.

Van De Sande, E. and Smith, J.M., "Surface Entrainment of Air by High Velocity Water Jets," *Chem. Eng. Sci.*, Vol. 28, 1161, 1973.

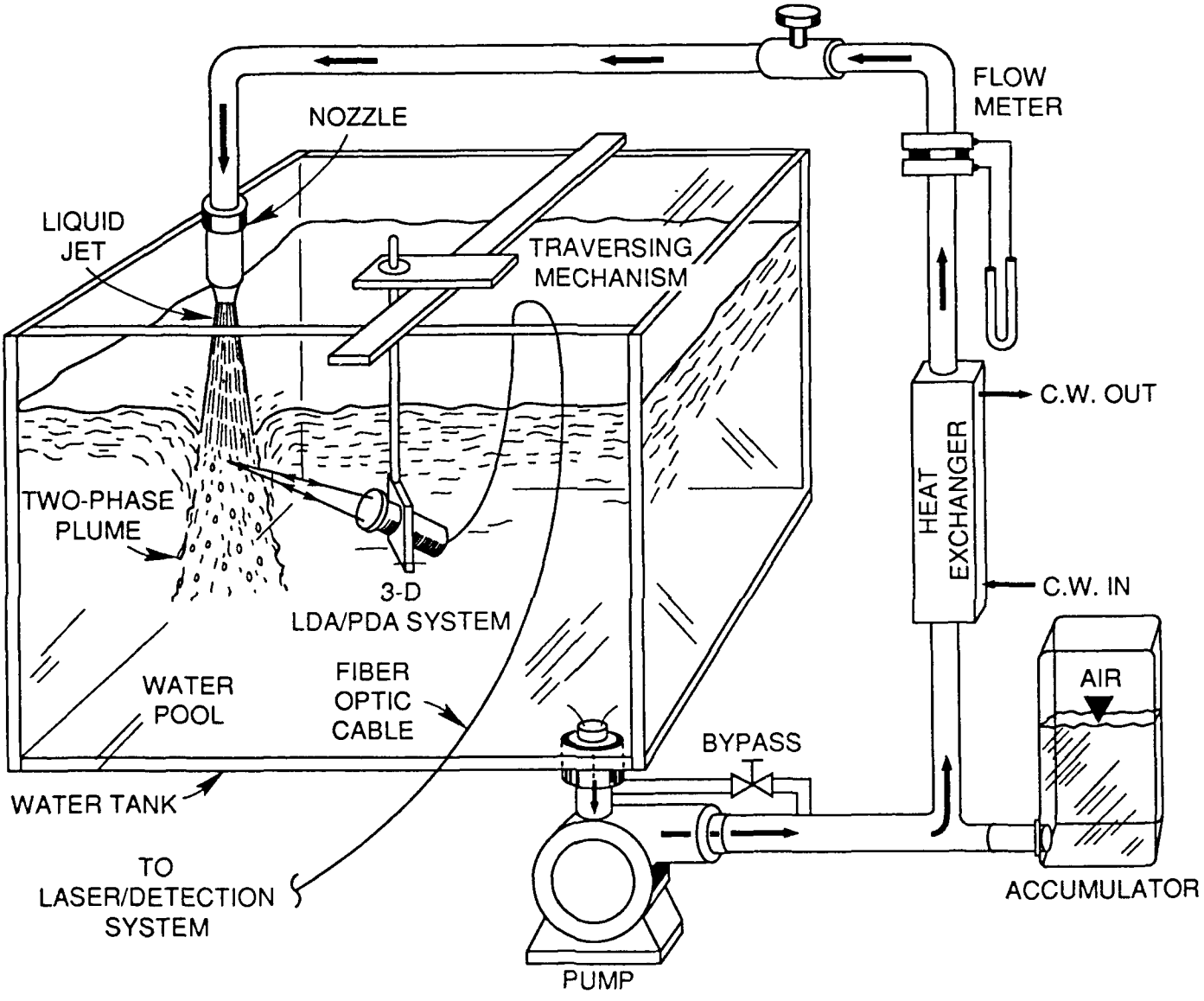

Figure 1 **Schematic of the Experimental Apparatus**

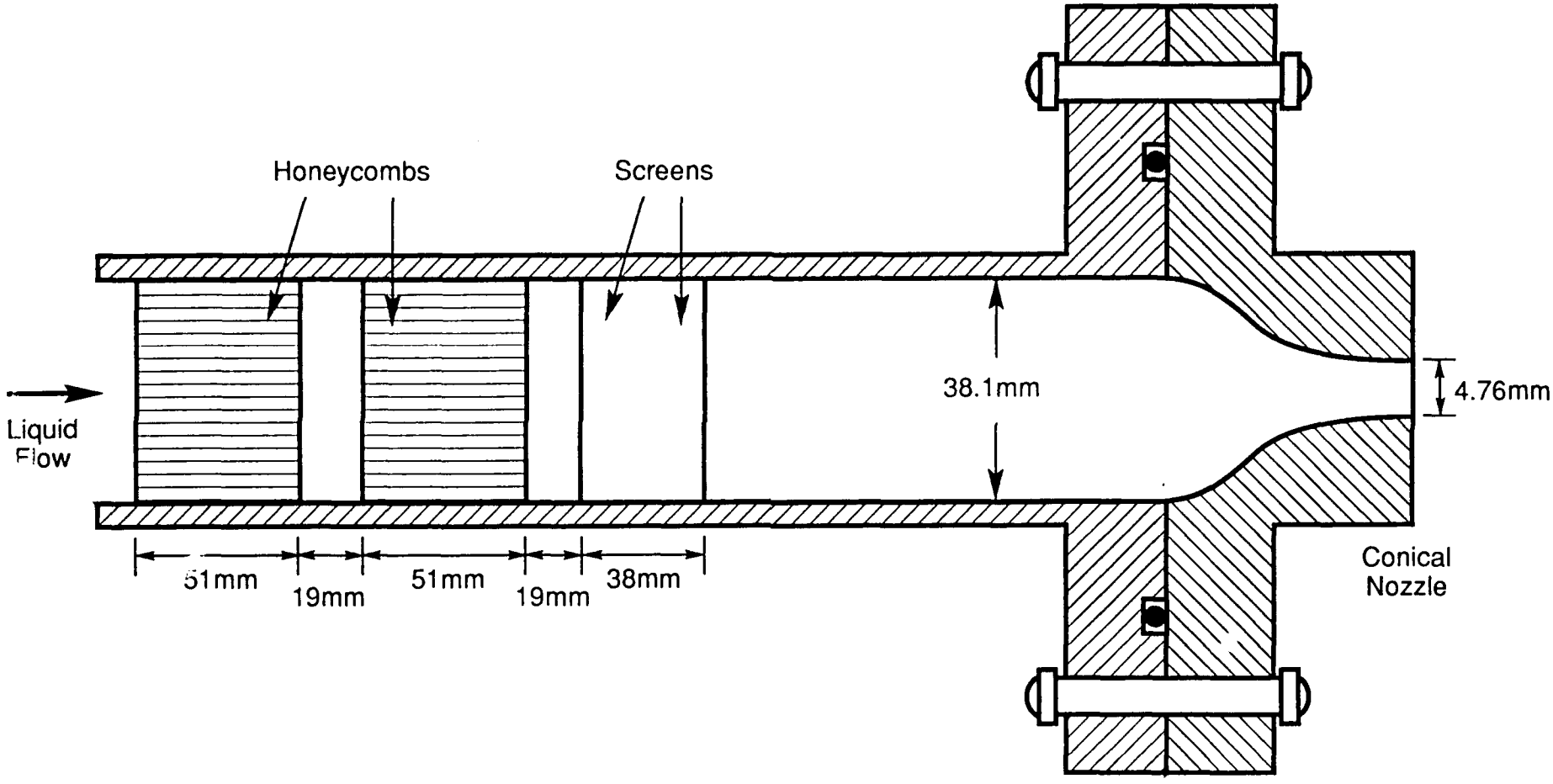

Figure 2 Schematic of the Conical Nozzle

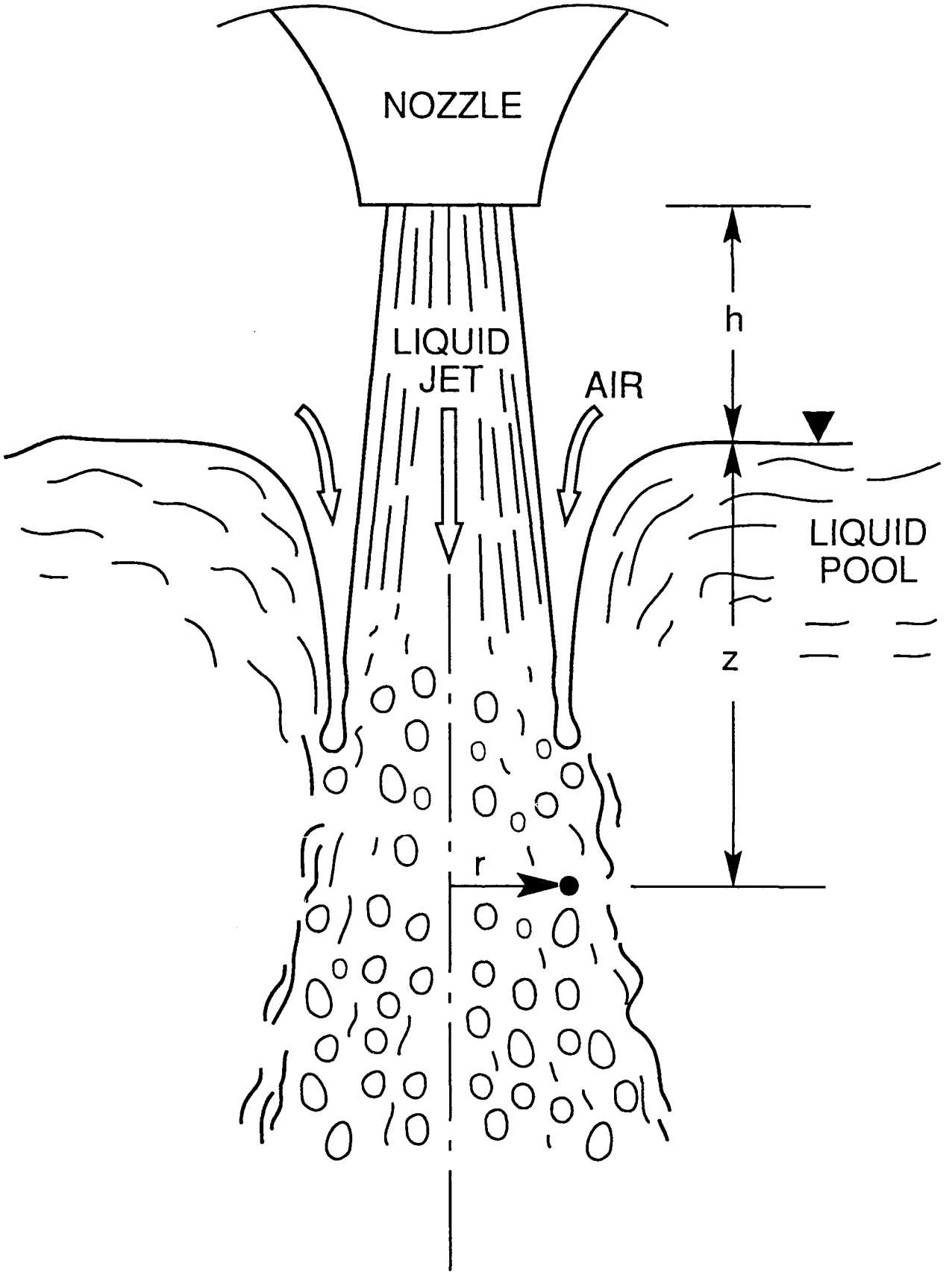

Figure 3 Schematic of the Air Entrainment Process

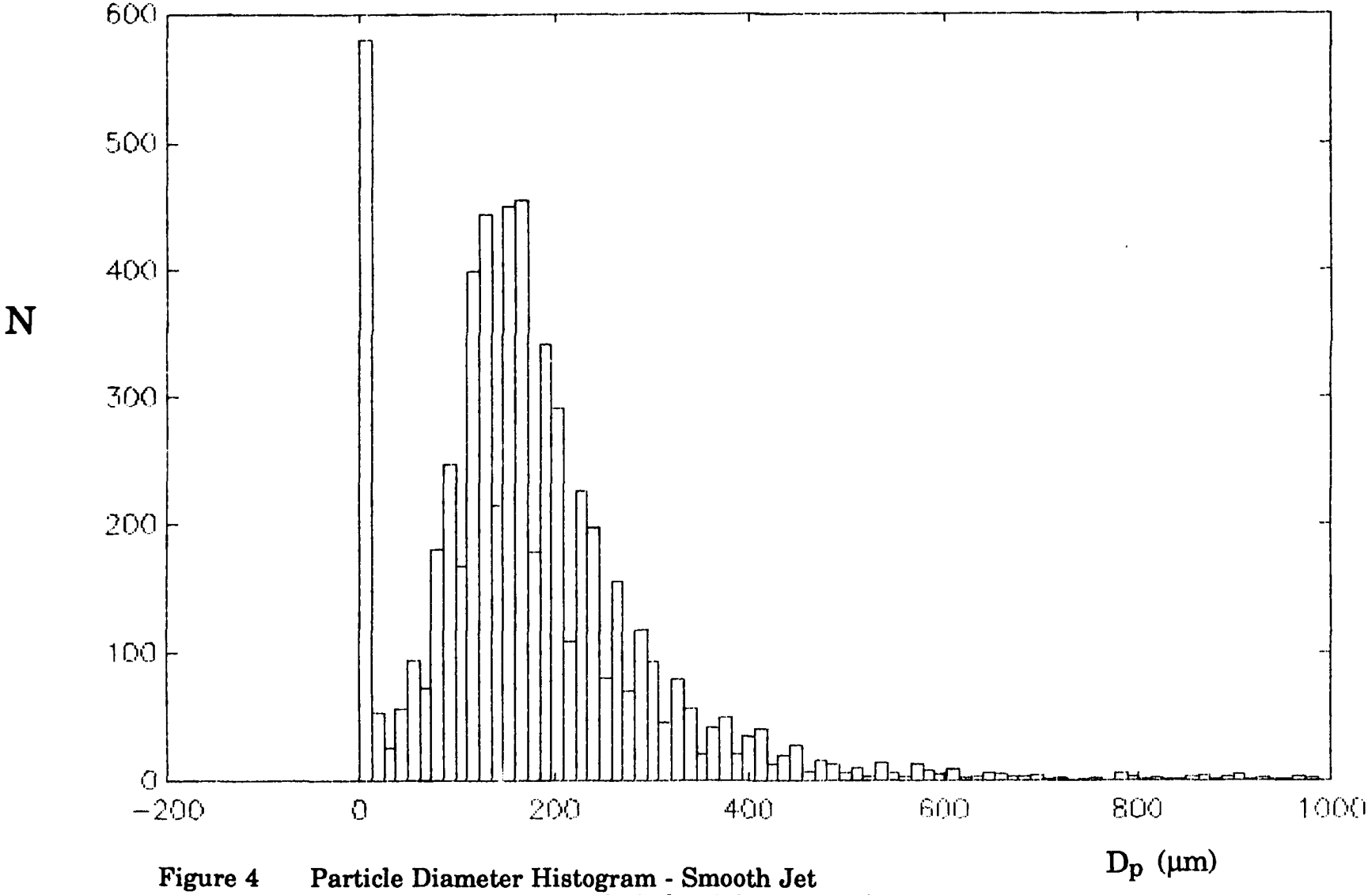

Figure 4 Particle Diameter Histogram - Smooth Jet
($z = 35.1$ mm; $w_\ell = 0.143$ kg/s; $h = 9.0$ mm, $r = 0$)

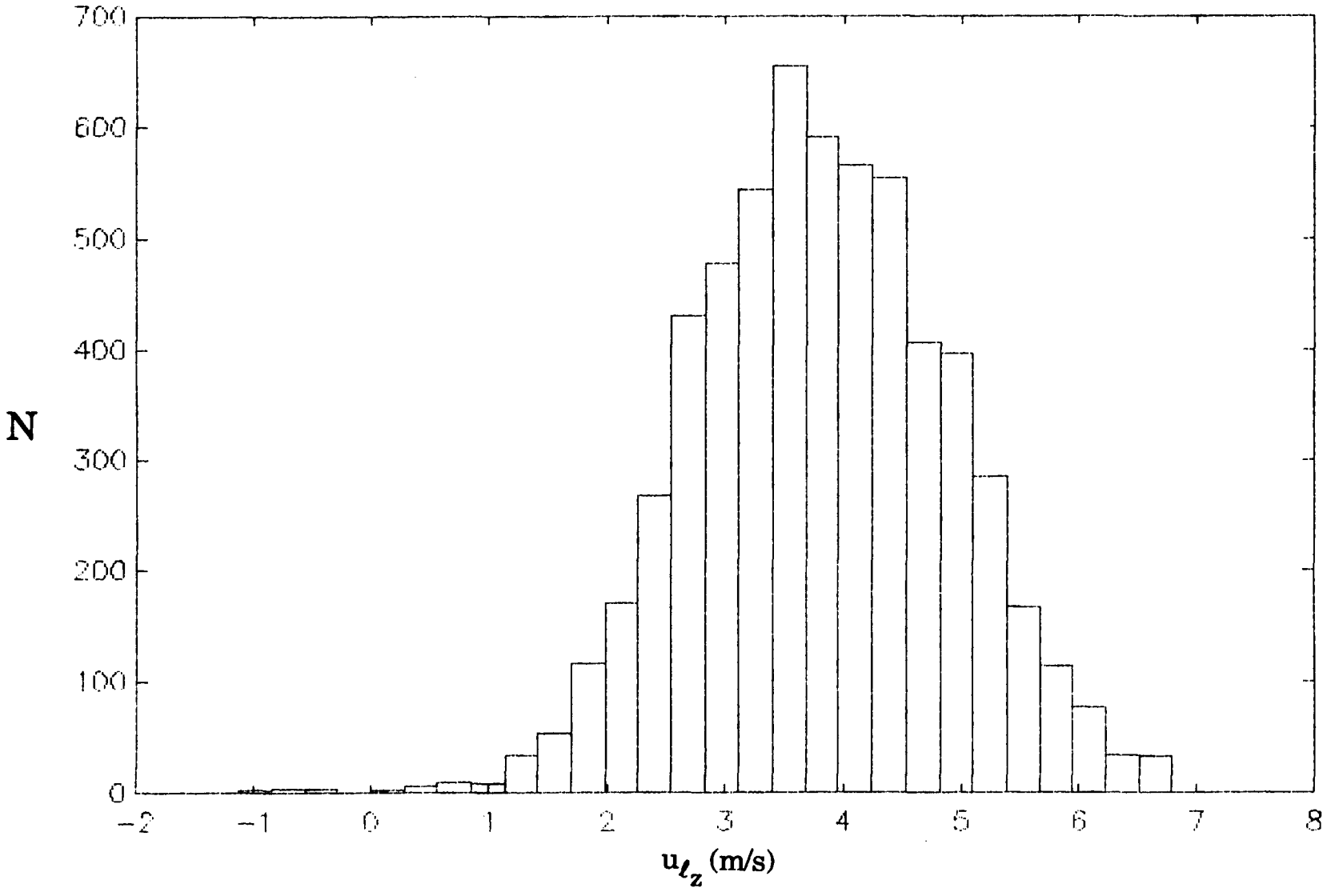

Figure 5 Liquid Velocity (d_p > 20 μm) Histogram - Smooth Jet
(z = 35.1 mm; w_ℓ = 0.143 kg/s; h = 9.0 mm; r = 0)

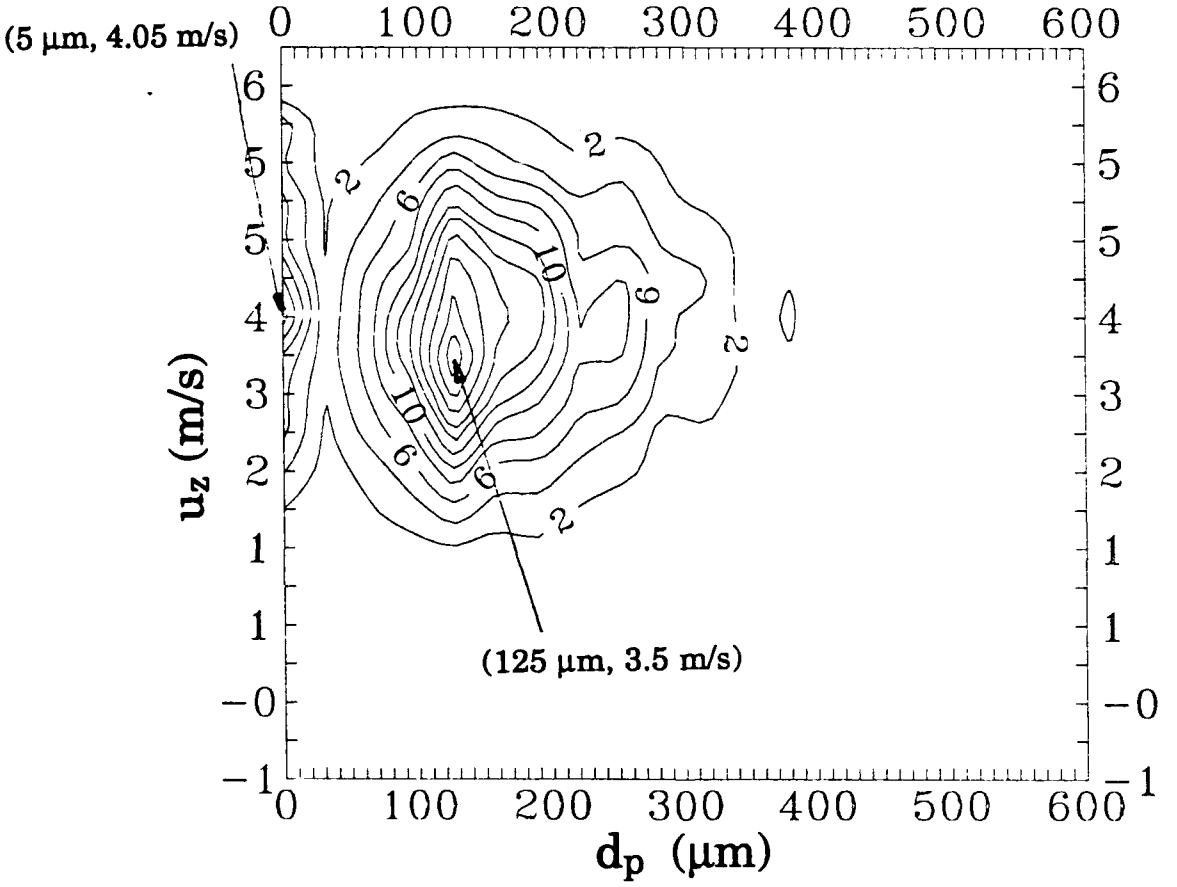

Figure 6a Contour Plot of the Two-Dimensional Probability Density Function - Smooth Jet (z = 35.1 mm; w_ℓ = 0.143 kg/s; h = 9.0 mm; r = 0)

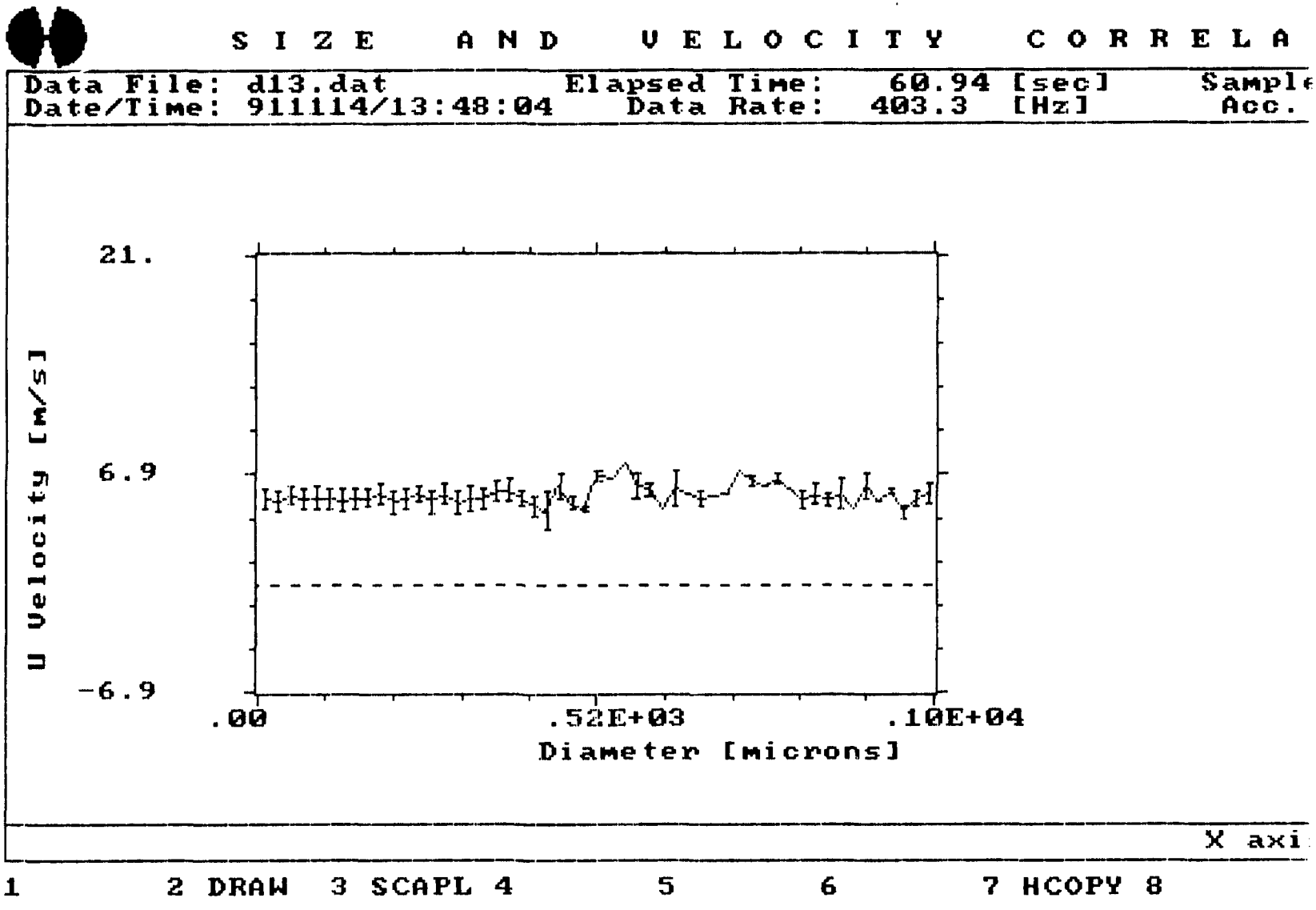

Figure 6b Mean Velocity (Continuous Line) and rms Fluctuation (error bars) as a Function of the Particle Diameter - Smooth Jet
(z = 35.1 mm; w_ℓ = 0.143 kg/s; h = 9.0 mm; r = 0)

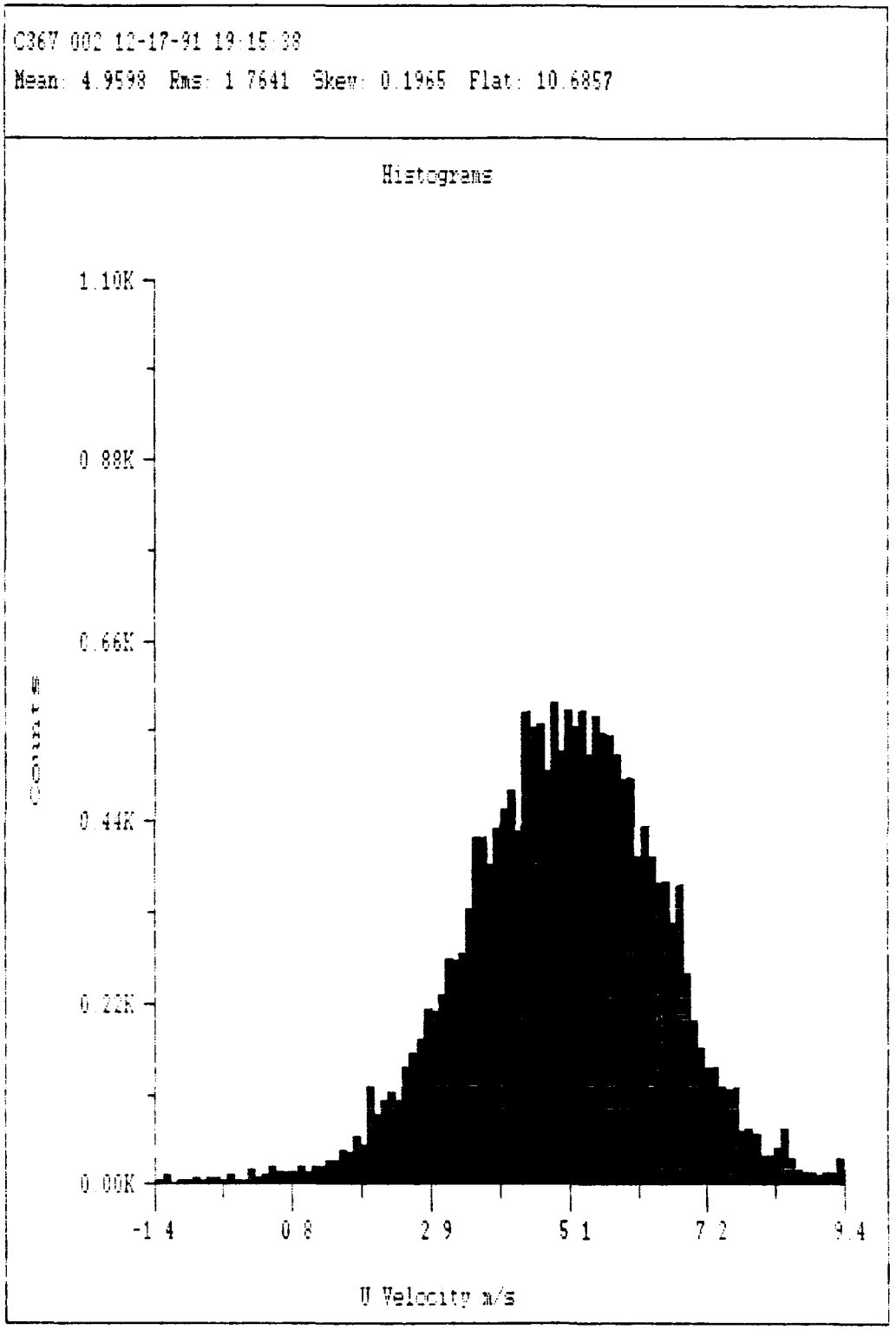

Figure 7 Liquid Velocity Histogram - Rough Jet
($z = 33$ mm; $w_\ell = 0.144$ kg/s; $h = 29.9$ mm; $r = 0$)

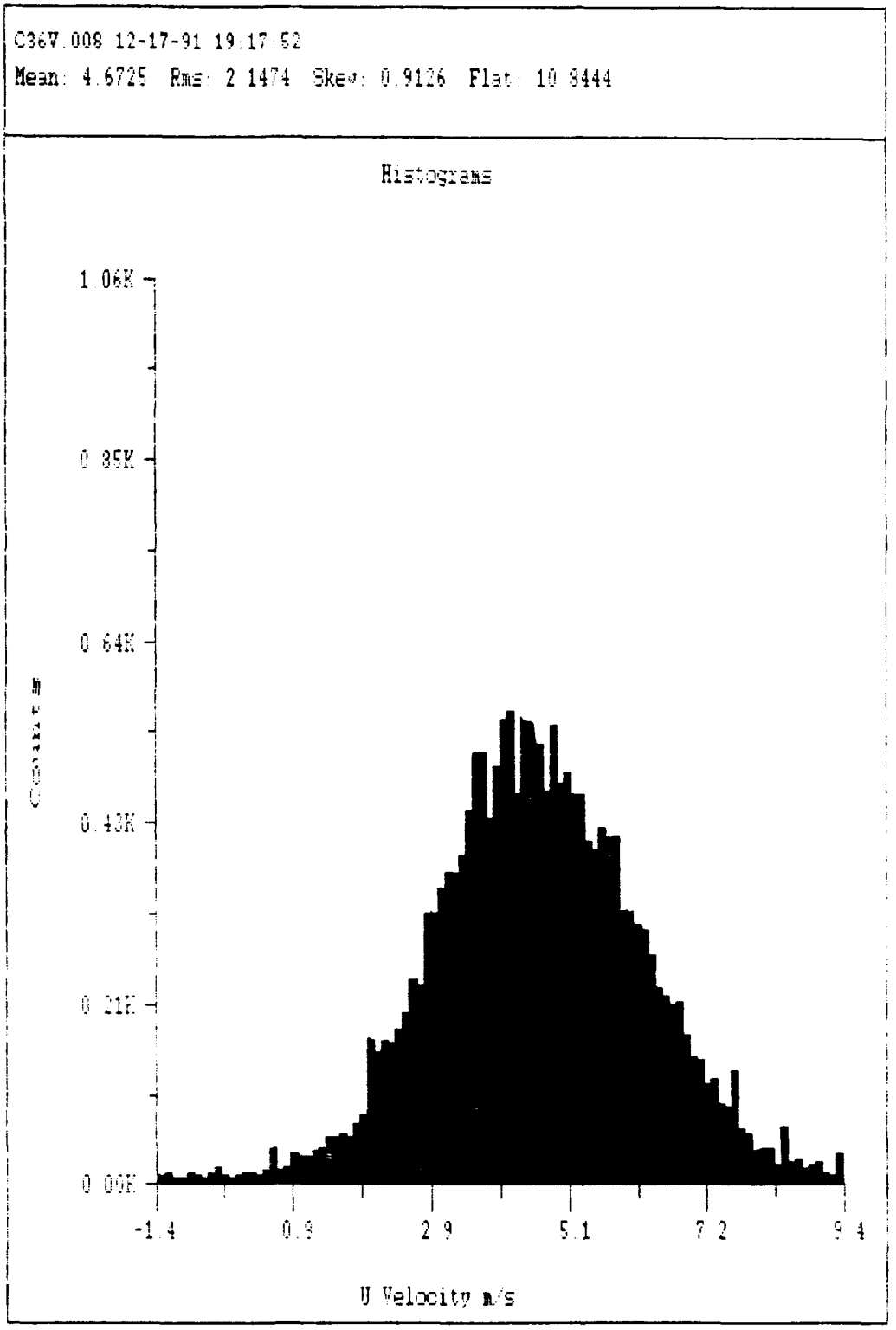

Figure 8 Gas Velocity Histogram - Rough Jet
($z = 33$ mm; $w_\ell = 0.144$ kg/s; $h = 29.9$ mm; $r = 0$)

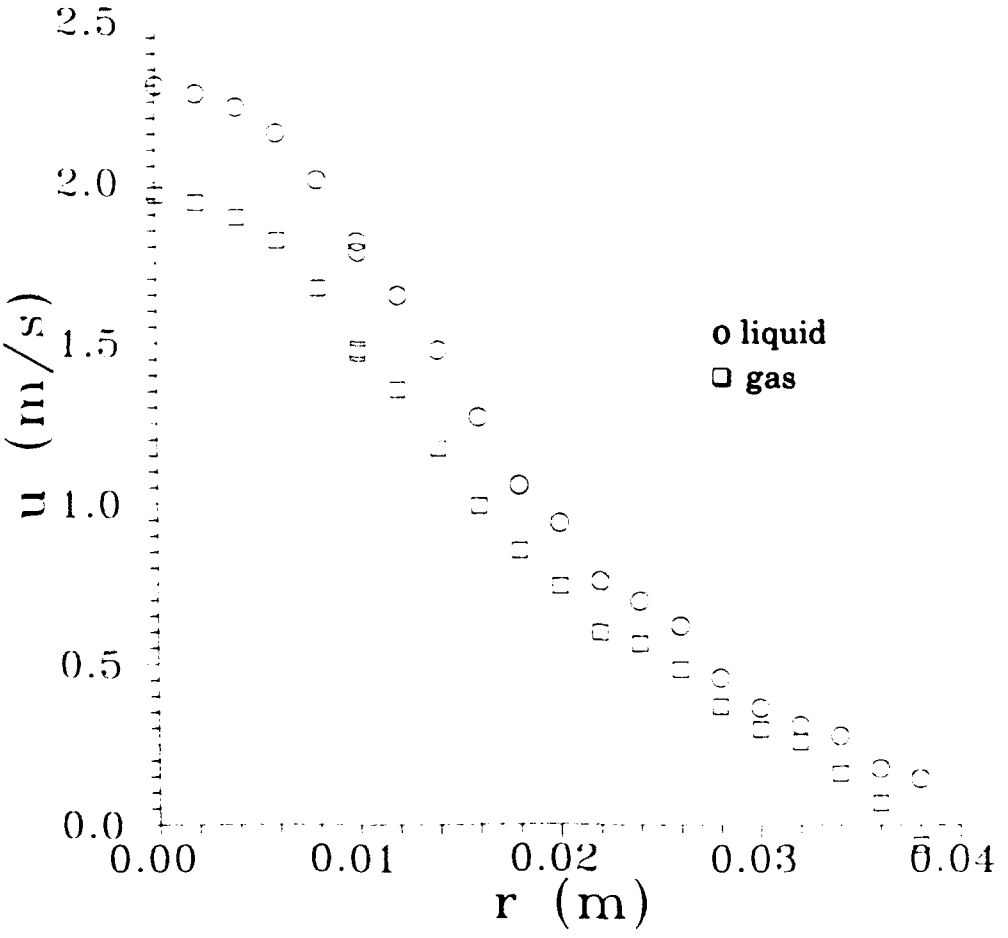

Figure 9 Liquid and Gas Mean Velocities as a Function of the Radial Distance - Rough Jet (z = 50.0 mm; w_ℓ = 0.125 kg/s; h = 17.3 mm)

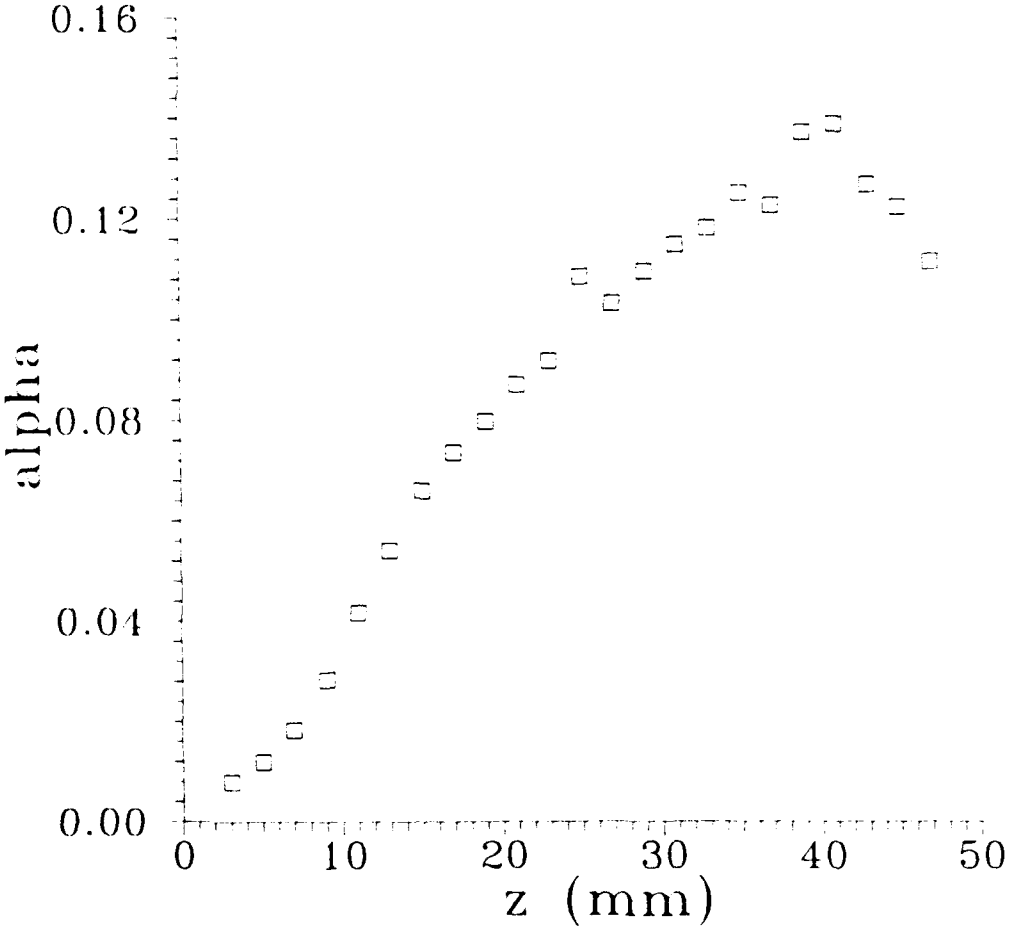

Figure 10 Void Fraction as a Function of the Distance beneath the Undisturbed Pool Level - Rough Jet (w_ℓ = 0.181 kg/s; h = 30 mm; r = 0)

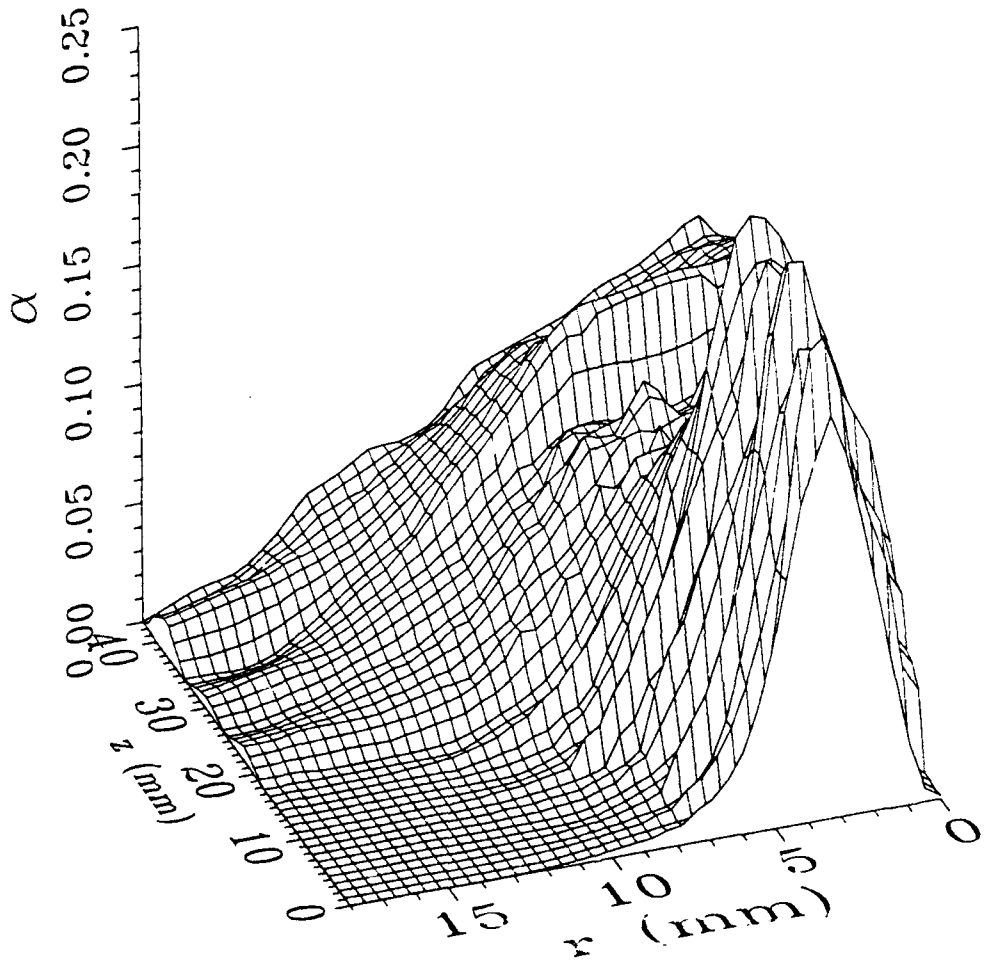

Figure 11 Void Fraction as a Function of r and z - Rough Jet

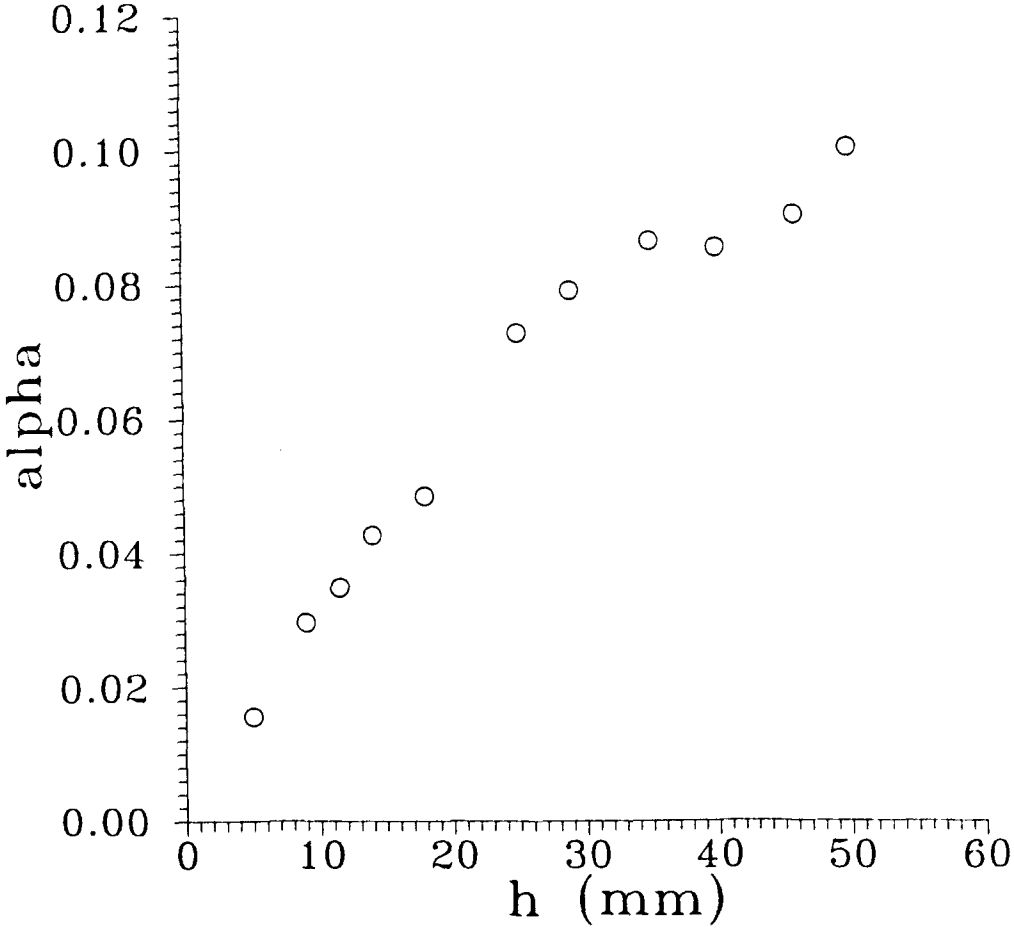

Figure 12 Void Fraction as a Function of the Distance from Nozzle Exit to the Undisturbed Water Level - Rough Jet
(w_f = 0.127 kg/s; h = 30 mm; z = 35 mm; r = 0)